ELSEVIER

Journal of Alloys and Compounds 275–277 (1998) 549–555

Journal of ALLOYS AND COMPOUNDS

Antiferromagnetic and quadrupolar interactions in rare-earth intermetallics

M. Amara*, P. Morin

Laboratoire Louis-Néel, C.N.R.S., BP 166X, 38042 Grenoble cedex, France

[1]

Abstract

NdZn and DyCu are two compounds (CsCl-type) illustrating the effects of high-order pair interactions on magnetic structures. They both display multiaxial orderings resulting in complex (H, T) phase diagrams. These diagrams are established using magnetization measurements on single crystals, neutron diffraction being the tool for determining the magnetic structures. For NdZn the calculations, including the quadrupolar couplings, give an accurate description of the magnetic order range. In DyCu, the magnetic multiaxial structures result from antiferroquadrupolar couplings, but to apprehend the (H, T) phase sequence needs the consideration of additional couplings.

Keywords: Magnetic structure; Quadrupolar interactions; Magnetic phase diagram

1. Introduction

Rare earth intermetallic compounds present a large variety of antiferromagnetic structures, which result from the coexistence of two-ion and one-ion interactions [1]. For lattices in which the rare-earth ions are at sites possessing multiple *n*-fold symmetry axes, the magnetic ground state is degenerate if only the crystal-field anisotropy and the RKKY bilinear interactions are considered. The actual magnetic structure is determined by high-order pair interactions, the most frequent ones being established to be of quadrupolar type [2]. These quadrupolar interactions are large for the cubic rare earth compounds RAg, RCu, RCd, RZn, which have the CsCl-type structure. Although these couplings are, in most cases, dominated by the bilinear ones, they remain active in selecting the most energetically favourable magnetic structure [3]. As illustrative examples of the stabilization of multiaxial magnetic structures by quadrupolar interactions, we present the results obtained in the study of the magnetic order range for the compounds NdZn and DyCu.

NdZn antiferromagnetically orders at $T_N = 70$ K [4]. The powder neutron diffraction patterns can be indexed with the hypothesis of an unique $\langle 1/2\ 0\ 0 \rangle$ propagation vector and with a moment directed along the *c* axis of the magnetic cell. A clear anomaly in the temperature variation of the magnetic susceptibility indicates a change of the magnetic structure at $T_R = 18.1$ K, the temperature at which specific heat measurements reveal a first-order transition [5].

DyCu antiferromagnetically orders at $T_N = 62$ K. Its neutron powder diffraction pattern is analysed using propagation vectors from the $\langle 1/2\ 1/2\ 0 \rangle$ star [6]. From CEF analysis and considering the absence of any evident strain below T_N, the spontaneous magnetic structure has been proposed as triple-*k*, the spins pointing along threefold axes [7].

In order to check the influence of the quadrupolar interactions in NdZn and DyCu, we have investigated their ordered range by means of magnetization and neutron diffraction measurements on single crystals, for magnetic fields applied along the [0 0 1], [1 1 1] and [1 1 0] axes. In the case of NdZn, we show the efficiency of the molecular periodic field method [8] for treating models simultaneously involving different kinds of pair interactions.

2. Multiaxial magnetic structures and quadrupolar interactions

The most frequently used Hamiltonian for describing the properties of rare-earth intermetallic compounds includes the Crystal Electric Field (CEF), bilinear interactions and Zeeman terms [2]. The bilinear interaction term is usually treated through a molecular field approximation. Looking for the magnetic structure which minimizes the free

*Corresponding author.

[1] Associated with the University Joseph-Fourier of Grenoble.

0925-8388/98/$19.00
PII: S0925-8388(98)00389-2

energy, one finds that it should satisfy a number of physical conditions:

– the antiferromagnetic propagation vectors belong to an unique star (in the cases of NdZn and DyCu, respectively $\langle 1/2\ 0\ 0\rangle$ and $\langle 1/2\ 1/2\ 0\rangle$),
– the magnetic moments' directions belong to a $\langle 1\ 0\ 0\rangle$, $\langle 1\ 1\ 0\rangle$ or $\langle 1\ 1\ 1\rangle$ cubic star,
– the magnetic moments' modulus is the same for all the magnetic sites of the crystal.

These conditions tend to satisfy the minimization of the bilinear exchange energy, according to the magnetic anisotropy. For a particular point of the Brillouin zone, which is in general a high symmetry point on the zone boundary, the Fourier transform of the bilinear coupling is maximum thus corresponding to a minimum for the interaction energy. This determines the involved star of antiferromagnetic propagation vectors, the uniqueness of which is generally confirmed by the experiments. Minimizing the energy also requires the magnetic moments to be maximum: the CEF terms of the Hamiltonian determine the axis of easy magnetization $\langle 1\ 0\ 0\rangle$, $\langle 1\ 1\ 0\rangle$ or $\langle 1\ 1\ 1\rangle$ in cubic symmetry. As we deal here with a simple cubic lattice, all the magnetic sites are equivalent and should equally contribute to the energy by all carrying the same moment modulus. In the case of structures induced by a magnetic field, these conditions are maintained except for the presence of an additional ferromagnetic component.

Actually, these conditions are not totally selective; there always exists more than one satisfactory model of structure. In particular, it can be seen that a collinear and a multiaxial structure, complying with the same anisotropy and periodicity conditions, would have the same free energy. To lower this degeneracy, one needs a more accurate description of the magnetic interactions. The next terms of pair interactions to be involved are the quadrupolar ones. They account for the couplings between the 4f shells taken as aspherical objects (the quadrupoles), as well as the couplings between the quadrupoles and the lattice through the magnetoelastic terms [9]. We focus here on the quadrupolar interaction terms; using the molecular field approximation for a magnetic site located at $\boldsymbol{R}_i$, this term writes:

$$H_{quad} = -Q_{O_2^0}(\boldsymbol{R}_i)O_2^0 - 3Q_{O_2^2}(\boldsymbol{R}_i)O_2^2 - Q_{P_{xy}}(\boldsymbol{R}_i)P_{xy} - Q_{P_{yz}}(\boldsymbol{R}_i)P_{yz} - Q_{P_{zx}}(\boldsymbol{R}_i)P_{zx}$$

where the various $Q_O(\boldsymbol{R}_i)$ and $Q_P(\boldsymbol{R}_i)$ represent the quadrupolar fields associated with each quadrupolar component. For example:

$$Q_{O_2^0}(\boldsymbol{R}_i) = \sum_{\boldsymbol{k}} K^{\gamma}(\boldsymbol{k})O_{2\boldsymbol{k}}^0 e^{i\boldsymbol{k}\boldsymbol{R}_i}$$

$O_{2\boldsymbol{k}}^0$ is the Fourier quadrupolar component of $\langle O_2^0\rangle$ and $K^{\gamma}(\boldsymbol{k})$ is the Fourier transform of the quadrupolar couplings. Note that in cubic symmetry, the description of the quadrupolar couplings requires two dispersion curves, $K^{\gamma}(\boldsymbol{k})$ and $K^{\epsilon}(\boldsymbol{k})$, associated with each of the quadrupolar irreducible representations γ and ϵ.

Starting from a given magnetic structure, taking the quadrupoles as quadratically induced by the magnetic exchange field, the quadrupolar Fourier components may be formally expressed [3]. The quadrupolar first-order correction to the free energy is then deduced and, consequently, one can determine which kind of interactions favours the considered structure (in terms of $K^{\gamma}(\boldsymbol{k})$ and $K^{\epsilon}(\boldsymbol{k})$).

For a quantitative treatment of the quadrupolar interactions, the molecular periodic field method is well adapted. The total Hamiltonian is self-consistently diagonalised for each site of the magnetic cell. The self-consistent solution is then obtained, recalculating the molecular fields at every site till the convergence. The thermodynamical functions and other statistical variables (i.e. the magnetic and quadrupolar components) can be calculated for any value of temperature or applied magnetic field.

3. Magnetization as a probe of the phase diagrams

The magnetization measurements have been performed at the Laboratoire Louis-Néel by the extraction method. The temperature range of the measurements extend from 1.5 K to room temperature, in applied magnetic fields up to 16 T. The single crystals were cut from ingots prepared by the Bridgman technique. Isothermal and isofield measurements were carried out for the three main crystallographic directions ([0 0 1], [1 1 1] and [1 1 0] axes). Isothermal magnetization curves are particularly well suited for locating the transition lines displaying weak slopes on the (H, T) phase diagram, while the isofield curves are ideal for the nearly vertical lines. For a better accuracy in locating the transition points, the field or temperature derivatives of the magnetization are used.

3.1. Magnetic phase diagrams of NdZn

For the twofold direction of the magnetic field, the outline of the phase diagram appears through the isofield measurements (inset of Fig. 1): in fields lower than $\mu_0 H =$ 5 T, two transitions can be observed, one corresponding to T_N and the other to T_R. Above $\mu_0 H = 5$ T, the analysis of the temperature derivative gives evidence for two transitions; the higher one corresponds to the antiferromagnetic ordering, the lower one to a change of magnetic structure. At $\mu_0 H = 6.5$ T three transitions are observed.

For this same direction of the applied field, at temperatures lower than $T_R = 18.1$ K, the isothermal magnetization curves show only one step-like transition at about $\mu_0 H =$ 3.5 T (Fig. 1). This remains unchanged above T_R, except for an increase of the critical field, which reaches a value

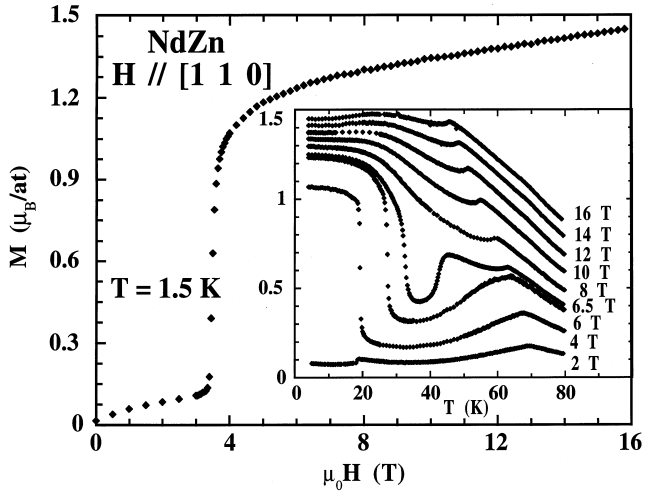

Fig. 1. Magnetization measurements on a NdZn single-crystal for a magnetic field applied along the [1 1 0] direction. The largest frame corresponds to the isothermal magnetization process at $T=1.5$ K. The inset shows the thermal evolution of the magnetization for different values of field.

$\mu_0 H=6.5$ T at about 40 K. At higher temperatures, this anomaly smoothes out and a second transition is visible as a change of the slope of the magnetization curve. For the threefold direction of the applied magnetic field, the isofield measurements are similar to those obtained along the twofold direction [10]. However, a clear difference of magnetization appears at low temperature between the $\mu_0 H=13$ and 14 T curves. The isothermal magnetization curves confirm that two step-like transitions, instead of one, exist for the threefold direction at low temperatures: the first one at about $\mu_0 H=4$ T and the second at $\mu_0 H=$ 13.5 T. In the case of the fourfold direction of the applied magnetic field, the isothermal magnetization curves (Fig. 2) displays two steps for low temperatures ($T<T_R$), at about $\mu_0 H=4.5$ and 9 T. Above T_R, only one step can be

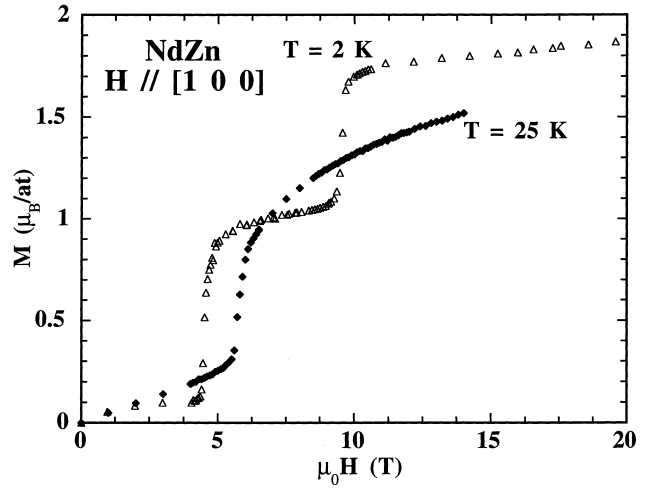

Fig. 2. Magnetization processes in NdZn along the [0 0 1] direction at 2 K and 25 K.

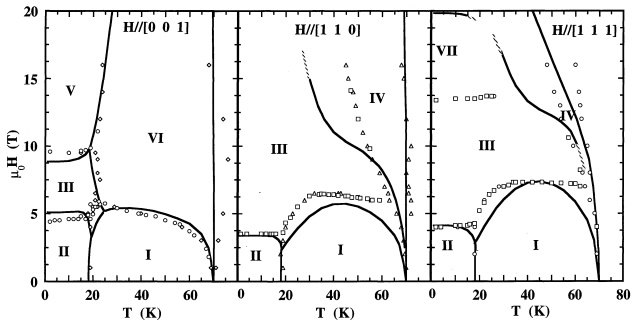

Fig. 3. Experimental and computed phase diagrams of NdZn.

observed. In Fig. 3 the magnetic phase diagrams resulting from the magnetization measurements for the three directions of the applied magnetic field are shown.

3.2. Magnetic phase diagrams of DyCu

For a field applied along a fourfold axis and just below $T_N=63$ K, the magnetization curves are nearly linear (Fig. 4, upper part). However, using the field derivative of the magnetization, two transitions can be resolved below $\mu_0 H=11$ T. Reducing the temperature, the amplitude of the anomalies is increased and the transitions clearly appear as steps on the magnetization curves: two successive transitions are observed for temperatures lower than 40 K. Looking at the isofield magnetization measurements, while decreasing the temperature at low field, the first anomaly, a change of slope, indicates the transition to-

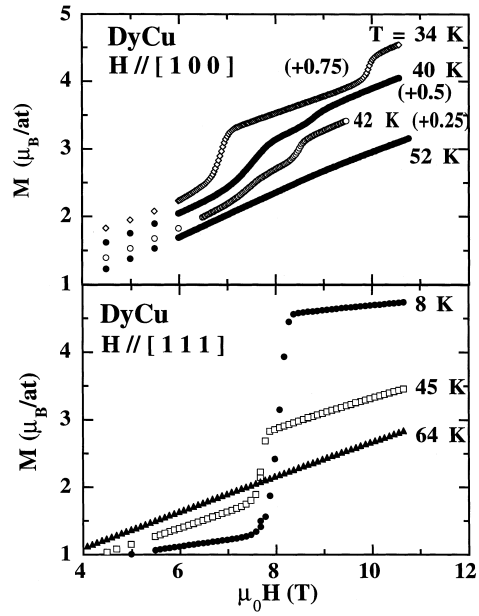

Fig. 4. Upper part, isothermal magnetization processes in DyCu along the [1 0 0] direction at $T=52$, 42, 40 and 34 K. The curves are shifted along the vertical axis according to the values in brackets. Lower part, isothermal magnetization processes in DyCu along the [1 1 1] direction at $T=64$, 45 and 8 K.

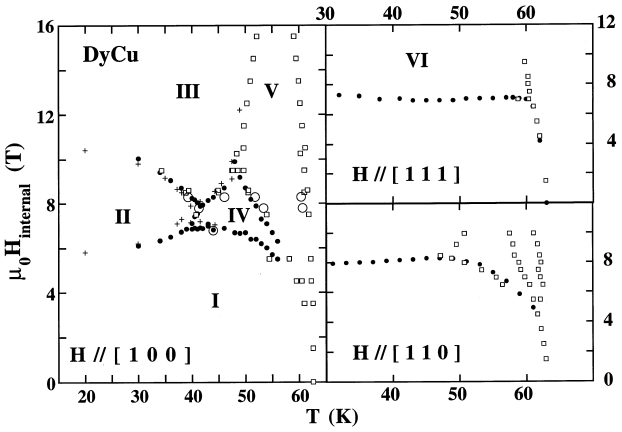

Fig. 5. Magnetic phase diagrams along the main crystallographic axes in DyCu. Open squares and black dots correspond to isofield and isothermal magnetization measurements, respectively. Circles correspond to neutron diffraction measurements.

wards the magnetic order [11]. At higher fields, additional transitions can be identified, again through changes in the magnetization slope.

Along the threefold direction, the isothermal magnetization processes present one single step for all accessible temperatures. While increasing the temperature, the amplitude of the magnetization jump progressively reduces down to zero about T_N (Fig. 4, lower part). Surprisingly, the associated critical field H_c appears as nearly temperature-insensitive, instead of decreasing with increasing temperature as in usual antiferromagnets. Measurements have also been carried out for a twofold direction of the applied magnetic field. They reveal a behaviour intermediate between the ones of the fourfold and threefold directions of the field. The phase diagrams for the fourfold, threefold and twofold direction of the applied magnetic field are plotted in Fig. 5.

4. Neutron diffraction determination of the magnetic structures

The neutron diffraction experiments were carried out on two spectrometers (both double axis with a moving up counter), DN3 at the C.E.N. Grenoble reactor Siloé and D15 at the I.L.L. The used cryomagnets could provide magnetic fields up to $\mu_0 H = 10$ T or $\mu_0 H = 6$ T at variable temperature.

The first step was to check that the spontaneous structures were effectively multiaxial. This is achieved by measuring the thermal dependence under an applied magnetic field of magnetic reflections associated with each branch of the star of propagation vectors. Domain effects are then clearly revealed, giving information on the symmetry of the magnetic structure. For instance, a triple-*k* structure, with moments along threefold axes, preserves the cubic point-group symmetry: no domain effect can result from such a structure. The main part of these experiments consists of measuring large sets of integrated intensities in each of the accessible phases. These intensities are then compared with the ones computed for structures which comply with the conditions given in Section 2. Starting from these conditions, the complete sets of so-called high symmetry magnetic structures may be established for a given star of propagation vectors [3,11]. These finite sets of models are used for the systematic analysis of neutron diffraction data measured on single crystals. With each model having a well defined symmetry, it is straightforward, using the elements of the cubic point-group, to determine the magnetic domains which must be considered. As they will all contribute to the neutron diffraction intensities, their relative proportions act as parameters for minimizing the reliability factor [12].

The results of the structure refinements for NdZn are given in Table 1. The structures are defined in terms of Fourier development, the $\boldsymbol{M}_\mu$ component being propagated by the $\boldsymbol{k}_\mu$ vector, and are shown in Fig. 6. The quadrupolar interaction analysis is summarized in the last column of Table 1. For instance, AFQ ϵ and FQ γ indicate that the structure is stable if the interactions are antiferroquadrupolar for the ϵ (Γ_3) quadrupolar irreducible representation (i.e. $K^\epsilon(\frac{1}{2}\frac{1}{2}0) > K^\epsilon(\mathbf{0})$) and ferroquadrupolar for the γ (Γ_5) representation (i.e. $K^\gamma(\mathbf{0}) > K^\gamma(\frac{1}{2}\frac{1}{2}0)$). For NdZn, the observed multiaxial structures demonstrate that the interactions are effectively AFQ ϵ and FQ γ. Note, that in the case of the $\langle 1/2\ 0\ 0\rangle$ antiferromagnetic propagation star, the field induced structures may also call in play quadrupolar propagation vectors from the $\langle 1/2\ 0\ 0\rangle$ star.

In Table 2 the multiaxial magnetic structures retained for DyCu's phases are given. The most coherent scheme is the one for which the moment directions are threefold in all phases and the interactions of the AFQ ϵ type. Note, that within this hypothesis, the transition between phases V and III is not explainable using models restricted to bilinear and quadrupolar pair interactions. The two phases, which are based on the same Fourier components, differ only through the relative layout between the propagation vectors and the propagated components. Actually, they would correspond to the same free energy. The structures corresponding to this most likely sequence with moments along threefold axes are represented in Fig. 7.

4.1. Description of NdZn's magnetic phase diagrams

This needs the prior knowledge of the CEF and bilinear interactions parameters of the Hamiltonian [9]. Thereafter, the difficulty is to obtain the values for the quadrupolar couplings, which are, except for the zone centre, impossible to measure directly. As results of the calculation within the periodic field method, the transitions between the different phases (i.e. the different structures) correspond to the crossings of the calculated free energies. In the case of NdZn, the values are optimized by adjusting the

Table 1
Fourier description of the magnetic structures associated with NdZn's phases. The first column gives the conditions of the neutron diffraction measurements. The labels refer to the real space structures represented in Figure 6. The fourth to sixth columns give, respectively, the number of domains involved in the refinement (N_{dom}), the amplitude of the moments ($|S|$) and the reliability factor (R). The seventh column gives the magnetization computed using $|S|$ for a rigid structure. The last column refers to the type of quadrupolar interactions compatible with the structure

Phase	Magnetic structure		Label	N_{dom}	R (%)	$\|S\|$ (μ_B)	M (μ_B)	Interactions
I	$\boldsymbol{M}_1=[1/\sqrt{3}\ 0\ 0]$	$\boldsymbol{k}_1=[1/2\ 0\ 0]$						
$T=25$ K	$\boldsymbol{M}_2=[0\ 1/\sqrt{3}\ 0]$	$\boldsymbol{k}_2=[0\ 1/2\ 0]$	t1	1	5.2	2.2	0	AFQ ϵ
$H=0$	$\boldsymbol{M}_3=[0\ 0\ 1/\sqrt{3}]$	$\boldsymbol{k}_3=[0\ 0\ 1/2]$						
II								
$T=3.7$ K	$\boldsymbol{M}_1=[1/\sqrt{2}\ 0\ 0]$	$\boldsymbol{k}_1=[1/2\ 0\ 0]$	d1	3	5.4	2.5	>0	AFQ ϵ
$\mu_0H=1.8$ T	$\boldsymbol{M}_2=[0\ 1/\sqrt{2}\ 0]$	$\boldsymbol{k}_2=[0\ 1/2\ 0]$						FQ γ
$\boldsymbol{H}\|[0\ 0\ 1]$								
III	$\boldsymbol{M}_0=[0\ 1/2\sqrt{2}\ 1/2\sqrt{2}]$	$\boldsymbol{k}_0=[0\ 0\ 0]$						
$T=2$ K	$\boldsymbol{M}_1=[1/\sqrt{2}\ 0\ 0]$	$\boldsymbol{k}_1=[1/2\ 0\ 0]$	Ht7	8	7.7	2.5	0.9	AFQ ϵ
$\boldsymbol{H}\|[0\ 0\ 1]$	$\boldsymbol{M}_2=[0\ 1/2\sqrt{2}\ -1/2\sqrt{2}]$	$\boldsymbol{k}_2=[0\ 1/2\ 0]$						
$\mu_0H=5.7$ T								
IV								
$T=61$ K	$\boldsymbol{M}_0=[1/\sqrt{3}\ -1/\sqrt{3}\ 0]$	$\boldsymbol{k}_0=[0\ 0\ 0]$	Hd8	1	9.2	0.9	0.45	FQ ϵ
$\boldsymbol{H}\|[1\ -1\ 0]$	$\boldsymbol{M}_1=[0\ 0\ 1/\sqrt{3}]$	$\boldsymbol{k}_1=[0\ 0\ 1/2]$						
$\mu_0H=7.9$ T								
V	$\boldsymbol{M}_0=[0\ 0\ 1/\sqrt{2}]$	$\boldsymbol{k}_0=[0\ 0\ 0]$		From quadrupolar interactions				AFQ ϵ
$\boldsymbol{H}\|[0\ 0\ 1]$	$\boldsymbol{M}_1=[1/\sqrt{2}\ 0\ 0]$	$\boldsymbol{k}_1=[1/2\ 0\ 0]$	Hd5	analysis				FQ γ
VI	$\boldsymbol{M}_0=[0\ 0\ 1/\sqrt{3}]$	$\boldsymbol{k}_0=[0\ 0\ 0]$		From joint neutron diffraction and				
$\boldsymbol{H}\|[0\ 0\ 1]$	$\boldsymbol{M}_1=[1/\sqrt{3}\ 0\ 0]$	$\boldsymbol{k}_1=[1/2\ 0\ 0]$	Ht1	quadrupolar interactions analysis				AFQ ϵ
	$\boldsymbol{M}_2=[0\ 1/\sqrt{3}\ 0]$	$\boldsymbol{k}_2=[0\ 1/2\ 0]$						
VII	$\boldsymbol{M}_0=[1/2\sqrt{2}\ 1/2\sqrt{2}\ 1/\sqrt{2}]$			From magnetization analysis				AFQ ϵ
$\boldsymbol{H}\|[1\ 1\ 1]$	$\boldsymbol{M}_1=[1/2\sqrt{2}\ -1/2\sqrt{2}\ 0]$	$\boldsymbol{k}_1=[0\ 1/2\ 0]$	Hd2					FQ γ

computed transition lines on the experimental ones (Table 3). As shown in Fig. 3, the result is satisfactory for the three directions of applied magnetic fields, in particular for the fourfold one.

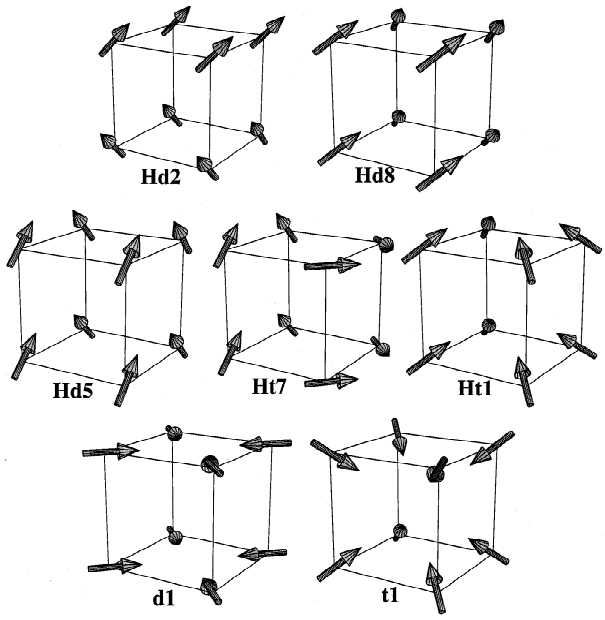

Fig. 6. Magnetic structures of NdZn. The labels refer to the Fourier descriptions given in Table 1.

5. Conclusion

The studies of NdZn and DyCu again point out the strong influence of the quadrupolar interactions in the rare-earth cubic compounds of the CsCl type. For NdZn, the molecular field description of the magnetic order range is in tight agreement with the experiment. All the observed multiaxial structures are reproduced and correctly located in the (H, T) phase diagrams.

If DyCu's sequence of multiaxial magnetic structures can be consistently explained as resulting from ϵ antiferroquadrupolar interactions, to understand its magnetic order range appears more delicate. The model which associates bilinear and quadrupolar interactions cannot explain some of the phase diagrams' features, in particular, the transition between phase III and V for the fourfold direction of the applied magnetic field. The origin may here be electronic. Indeed, the latent instability of the conduction band is well known in the RCu compounds with heavy rare-earths. It drives a martensitic-type lattice transition through a zone boundary mechanism with the same $\langle 1/2\ 1/2\ 0\rangle$ propagation vector as the magnetic one [13]. The lattice transition strongly depends on the lattice parameter and occurs around 180 K in paramagnetic GdCu, 140 K in YCu. It is triggered by the $\langle 1/2\ 1/2\ 0\rangle$ magnetic ordering at $T_N=115$ K in TbCu [14]. The cubic structure is stable in the other RCu, although to substitute

Table 2
Fourier description of the magnetic structures associated with DyCu's phases. The first column gives the conditions of the neutron diffraction measurements. The labels refer to the real space structures represented in Figure 7. The fourth to sixth columns give, respectively, the number of domains involved in the refinement (N_{dom}), the amplitude of the moments ($|S|$) and the reliability factor (R). The seventh column gives the magnetization computed using $|S|$ for a rigid structure. The last column refers to the type of quadrupolar interactions compatible with the structure

Phase	Magnetic structure		Label	N_{dom}	R (%)	$\|S\|$ (μ_B)	M (μ_B)	Interactions
I	$\boldsymbol{M}_1=[1/\sqrt{3}\ 0\ 0]$	$\boldsymbol{k}_1=[0\ 1/2\ 1/2]$						
$T=10$ K	$\boldsymbol{M}_2=[0\ 1/\sqrt{3}\ 0]$	$\boldsymbol{k}_2=[1/2\ 0\ 1/2]$	I_t	1	6.9	9.4	0	AFQ ϵ
$H=0$	$\boldsymbol{M}_3=[0\ 0\ 1/\sqrt{3}]$	$\boldsymbol{k}_3=[1/2\ 1/2\ 0]$						
II	$\boldsymbol{M}_0=[0\ 0\ 1/2\sqrt{3}]$	$\boldsymbol{k}_0=[0\ 0\ 0]$						
$T=2$ K	$\boldsymbol{M}_1=[1/\sqrt{3}\ 0\ 1/2\sqrt{3}]$	$\boldsymbol{k}_1=[1/2\ 0\ 1/2]$	II_t	4	8.1	9.3	2.7	AFQ ϵ
$\boldsymbol{H}\|[0\ 0\ 1]$	$\boldsymbol{M}_2=[0\ 0\ -1/2\sqrt{3}]$	$\boldsymbol{k}_2=[1/2\ 1/2\ 0]$						
$\mu_0H=7.5$ T	$\boldsymbol{M}_3=[0\ 1/\sqrt{3}\ 1/2\sqrt{3}]$	$\boldsymbol{k}_3=[0\ 1/2\ 1/2]$						
III	$\boldsymbol{M}_0=[0\ 0\ 1/\sqrt{3}]$	$\boldsymbol{k}_0=[0\ 0\ 0]$						
$T=44$ K	$\boldsymbol{M}_1=[0\ 1/\sqrt{3}\ 0]$	$\boldsymbol{k}_1=[0\ 1/2\ 1/2]$	III_t	1	11.4	8.2	4.7	AFQ ϵ
$\mu_0H=8.3$ T	$\boldsymbol{M}_2=[1/\sqrt{3}\ 0\ 0]$	$\boldsymbol{k}_2=[1/2\ 0\ 1/2]$						
	$\boldsymbol{M}_0=[0\ 1/2\sqrt{2}\ 1/2\sqrt{2}]$	$\boldsymbol{k}_0=[0\ 0\ 0]$						
IV	$\boldsymbol{M}_1=[1/\sqrt{2}\ 0\ 0]$	$\boldsymbol{k}_1=[0\ 1/2\ 1/2]$	IV_b	8	10.8	7	2.5	AFQ ϵ
$T=48$ K	$\boldsymbol{M}_2=[0\ 1/2\sqrt{2}\ -1/2\sqrt{2}]$	$\boldsymbol{k}_2=[1/2\ 0\ 1/2]$						AFQ γ
$\boldsymbol{H}\|[0\ 0\ 1]$								
$\mu_0H=8.3$ T	$\boldsymbol{M}_0=[0\ 0\ 1/2\sqrt{3}]$	$\boldsymbol{k}_0=[0\ 0\ 0]$						
	$\boldsymbol{M}_1=[1/\sqrt{3}\ 0\ 1/2\sqrt{3}]$	$\boldsymbol{k}_1=[0\ 1/2\ 1/2]$	IV_t	4	14.6	6.1	1.8	AFQ ϵ
	$\boldsymbol{M}_2=[0\ 0\ -1/2\sqrt{3}]$	$\boldsymbol{k}_2=[1/2\ 1/2\ 0]$						
	$\boldsymbol{M}_3=[0\ 1/\sqrt{3}\ 1/2\sqrt{3}]$	$\boldsymbol{k}_3=[1/2\ 0\ 1/2]$						
	$\boldsymbol{M}_0=[0\ 0\ 1/\sqrt{3}]$	$\boldsymbol{k}_0=[0\ 0\ 0]$						
V	$\boldsymbol{M}_1=[1/\sqrt{3}\ 0\ 0]$	$\boldsymbol{k}_1=[0\ 1/2\ 1/2]$	V_t	1	11.3	5.8	3.3	AFQ ϵ
$T=53$ K	$\boldsymbol{M}_2=[0\ 1/\sqrt{3}\ 0]$	$\boldsymbol{k}_2=[1/2\ 0\ 1/2]$						
$\boldsymbol{H}\|[0\ 0\ 1]$								
$\mu_0H=8.3$ T	$\boldsymbol{M}_0=[0\ 0\ 1/\sqrt{2}]$	$\boldsymbol{k}_0=[0\ 0\ 0]$	V_b	2	11.3	6.7	4.7	AFQ ϵ
	$\boldsymbol{M}_1=[1/\sqrt{2}\ 0\ 0]$	$\boldsymbol{k}_1=[0\ 1/2\ 1/2]$						FQ γ
	$\boldsymbol{M}_0=[1/4\sqrt{2}\ 1/4\sqrt{2}\ 1/2\sqrt{2}]$	$\boldsymbol{k}_0=[0\ 0\ 0]$						
	$\boldsymbol{M}_1=[3/4\sqrt{2}\ 3/4\sqrt{2}\ -1/2\sqrt{2}]$	$\boldsymbol{k}_1=[1/2\ 1/2\ 0]$	VI_b	3	7.6	8.1	3.3	AFQ γ
VI	$\boldsymbol{M}_2=[1/4\sqrt{2}\ -1/4\sqrt{2}\ 0]$	$\boldsymbol{k}_2=[0\ 1/2\ 1/2]$						AFQ ϵ
$T=40$ K	$\boldsymbol{M}_3=[-1/4\sqrt{2}\ 1/4\sqrt{2}\ 0]$	$\boldsymbol{k}_3=[1/2\ 0\ 1/2]$						
$\boldsymbol{H}\|[1\ 1\ 1]$								
$\mu_0H=8.3$ T	$\boldsymbol{M}_0=[1/2\sqrt{3}\ 1/2\sqrt{3}\ 1/2\sqrt{3}]$	$\boldsymbol{k}_0=[0\ 0\ 0]$						
	$\boldsymbol{M}_1=[1/2\sqrt{3}\ 1/2\sqrt{3}\ -1/2\sqrt{3}]$	$\boldsymbol{k}_1=[1/2\ 1/2\ 0]$	VI_t	1	7.6	8.5	4.25	AFQ ϵ
	$\boldsymbol{M}_2=[-1/2\sqrt{3}\ 1/2\sqrt{3}\ 1/2\sqrt{3}]$	$\boldsymbol{k}_2=[0\ 1/2\ 1/2]$						
	$\boldsymbol{M}_3=[1/2\sqrt{3}\ -1/2\sqrt{3}\ 1/2\sqrt{3}]$	$\boldsymbol{k}_3=[1/2\ 0\ 1/2]$						

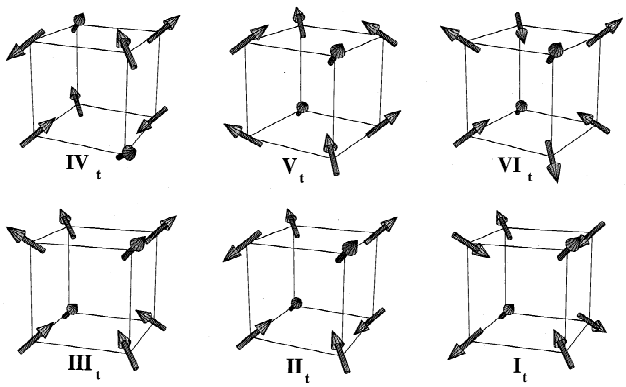

Fig. 7. Magnetic structures of DyCu, with moments along threefold axes, as determined from the neutron diffraction measurements. The labels relate the structures with the Fourier descriptions given in Table 2.

10% of Ho ions with Y ones reintroduces the instability at 80 K in HoCu [15]. In DyCu, cubic in the spontaneous state, the magnetic field acting as an external stress may modify the electronic properties, thus the strength of the various magnetic couplings and the logical sequence of the field-induced structures. This is illustrative of the complexity of the interactions which are responsible for the order range properties in rare-earth intermetallic compounds.

Table 3
The quadrupolar interactions constants used for describing NdZn's phase diagrams

$\boldsymbol{k}$	0	[1/2 0 0]	[1/2 1/2 0]
$K^{\gamma}(\boldsymbol{k})$ (K)	−0.088	−0.070	−0.100
$K^{\epsilon}(\boldsymbol{k})$ (K)	0	0.410	0.207

Taking account of the quadrupolar interactions substantially lifts the degeneracy between the many high symmetry models which comply with the same magnetic-anisotropy and periodicity requirements. Thus, the sequence of multiaxial (or collinear) magnetic structures can be coherently interpreted, although it doesn't realise a unique solution which could be unambiguously predicted.

References

[1] B. Coqblin, The Electronic Structure of Rare-Earth Metals and Alloys: The Magnetic Heavy Rare Earths, Academic Press, New York, 1977.
[2] P. Morin, D. Schmitt, in: K.H.J. Buschow, E.P. Wohlfarth (Eds.), Ferromagnetic Materials, North-Holland, vol. 5, Amsterdam, 1990, p. 1.
[3] M. Amara, P. Morin, Physica B 205 (1995) 379.
[4] P. Morin, J. Pierre, Phys. Status Solidi A 30 (1975) 549.
[5] P. Morin, A. de Combarieu, Solid State Commun. 17 (1975) 975.
[6] M. Wintenberger, R. Chamard-Bois, M. Belakhovsky, J. Pierre, Phys. Status Solidi B 48 (1971) 705.
[7] R. Aléonard, P. Morin, J. Rouchy, J. Magn. Magn. Mater. 46 (1984) 233.
[8] J.A. Blanco, D. Gignoux, D. Schmitt, Phys. Rev. B 43 (1991) 13145.
[9] M. Amara, P. Morin, Physica B 222 (1996) 61–72.
[10] M. Amara, P. Morin, P. Burlet, Physica B 210 (1995) 157.
[11] M. Amara, P. Morin, F. Bourdarot, J. Phys. Condens. Matter 9 (1997) 7441.
[12] M. Amara, R.M. Galéra, P. Morin, J. Voiron, P. Burlet, J. Magn. Magn. Mater. 131 (1994) 402.
[13] I. Abu-Aljarayesh, J.S. Kouvel, T.O. Brun, Phys. Rev. B 34 (1986) 240.
[14] J. Pierre, B. Hennion, in: R.P. Guertin, W. Suski, Z. Zolmierek (Eds.), Crystalline Electric Fields Effects in f-Electrons Magnetism, Plenum, New York, 1982, p. 275.
[15] I. Abu-Aljarayesh, J.S. Kouvel, T.O. Brun, J. Magn. Magn. Mater. 54–57 (1986) 512.